Zigzag shaped magnetic sensors

F.C.S. da Silva[a], W.C. Uhlig[b], A.B. Kos[a], S. Schima[a], J. Aumentado[a], M.J. Donahue[b], J. Unguris[b], and D.P. Pappas[a]

National Institute of Standards and Technology

[a] *Boulder, Colorado 80305*

[b] *Gaithersburg, MD 20899*

(Dated: May 7, 2004)

Abstract

Magnetism in zigzag shaped thin film elements is investigated using scanning electron microscopy with polarization analysis, magneto-transport measurements, and micromagnetic simulations. We find that the angle of magnetization alternates along the length of the element, and is strongly correlated to the corrugated edges. We show that this simple and unique geometry can be used as a naturalo form a magnetic field sensor. In this configuration the sensors are primarily sensitive to fields parallel to the applied current. Our results can be interpreted in terms of a coherent rotation model of the magnetization. These devices are scalable to nanometer dimensions.

Recently, images of nanometer-scale magnetic structures suggested that the magnetization follows the contour of the edges [1]. An important extension of this work on 250 nm wide elements with serrated edges (zigzag shaped) [2] was demonstrated using Lorentz microscopy. In these elements, the magnetization was shown to exhibit an alternating pattern of easy axis orientations. To have control of the magnetization in this manner is of great importance in the development of scalable magnetoresistive (MR) sensors because more complicated current- and field-biasing schemes are not required, and nanoscale devices based on this technology have become increasingly important. For example, these types of devices have been instrumental in the data storage revolution that has occurred over the past decade [3]. Similar MR devices have also been used as high sensitivity sensors for current- [4–6] and magnetization-induced [7, 8] field imaging. A critical aspect of the design of these devices is the biasing of the magnetization and current flow in order to obtain an antisymmetric, linear response. In this letter we demonstrate a novel method of maintaining a bias between the magnetization and the current direction using the contour of the element.

In a single film anisotropic magnetoresistive (AMR) sensor, the resistance can be described by [9]

$$R = R_\circ + \Delta R \cos^2(\theta - \alpha), \tag{1}$$

where $R_\circ$ and ΔR are material-dependent constants ($\Delta R/R_\circ = 2 - 4$ % for Permalloy), θ and α are respectively the angles formed by the magnetization and the applied current directions with respect to the easy axis of the material. To obtain the desired response of the device versus the external magnetic field, H, several schemes to bias the magnetization relative to the direction of the current have been proposed. For example, in the barber-pole method [10] the angle of the current flow is set at $\alpha = 45^\circ$ and H is applied at an angle $\phi = 90^\circ$ with respect to the uniaxial easy axis of the film. The angle α is obtained with equally spaced electrical contacts at a 45° angle with respect to the magnetic easy axis of the element. In this configuration ($\alpha = 45^\circ$ and $\phi = 90^\circ$) the magnetization rotates coherently with the applied field, *i.e.*, $\cos\theta \propto H$ and, according to Eq. 1, the response of R with respect to H (the so called transfer curve) will be linear around zero field. To obtain a uniaxial magnetic element, it is common to choose a soft magnetic material and use both shape and induced anisotropies to ensure the existence of only one anisotropy axis. Therefore, elongated shapes are typically used, with attention to the geometrical shape of the ends to avoid magnetization curl and vortices[11].

Therefore, in this current work we fabricated single layer, elongated devices that have a zigzag shaped magnetic layer. The zigzag has a similar aspect ratios to those of Ref. [2], as shown in Fig. 1. The structures were fabricated using optical lithography and a lift-off process for both the magnetic and contact layers. A 30 nm thick magnetic layer was sputtered from a $Ni_{80}Fe_{20}$ target onto a SiO_2-coated Si wafer with an external field of 15 $kA{\cdot}m^{-1}$ applied along the long axis of the structure. Two 5 nm-thick Ta layers were deposited before and after the Permalloy layer. The Ta serves to texture and protect the magnetic layer. The Al contacts at the ends were electron-beam evaporated onto the magnetic element after a brief ion mill to remove the top Ta layer in that region.

Finite element analysis of the current flow in these devices shows that the current will primarily flow down the center of the element along the $\hat{\mathbf{x}}$ axis. The magnetic state in zero magnetic field was imaged using scanning electron microscopy with polarization analysis (SEMPA). SEMPA is a non-invasive, high spatial resolution ($<$ 15 nm) technique that measures the magnetization direction by analyzing the spin-polarization of the secondary electrons emitted from the sample in a scanning electron microscope [12, 13].

The micromagnetic simulations were performed using the Object Oriented MicroMagnetic Framework (OOMMF) [14–16]. OOMMF is a public domain program for micromagnetics that has been developed at NIST. Micromagnetics is a continuum model of three dimensional vector magnetization in ferromagnetic materials. The simulations in this paper compute equilibrium magnetization configurations, which correspond to minima in the energy landscape. The energy here consists of magnetostatic, exchange, and magneto-crystalline anisotropy components. The electrical transport measurements were obtained using a four-probe technique with the external magnetic field applied in the plane of the film (Fig. 1).

Figure 2a shows a SEMPA image of the magnetization of the zigzag structure for the remanent state obtained after the sample was saturated in the $\hat{\mathbf{x}}$ direction. Along the axis, we find parallelogram-shaped regions where the magnetization alternates direction along the axis, with domain walls spanning the element from each pair of opposing acute and obtuse angles. This pattern matches that observed in Ref [2] on nanoscale elements, demonstrating the scaling of this configuration. We also observe vortex structures near the ends of our devices. The presence of vortices depends on the saturation history of the sample. We find that they can be eliminated with a strong enough saturation field. However, the magnetization in the parallelograms tends to return, reversibly, back to the zero field values

after saturation. This is presumably because the domain walls are pinned at the corners of the structure. The average direction of the magnetization within each parallelogram alternates between $\pm 25^\circ$, in a zigzag fashion as shown in the scan across the center of the element in the $\hat{\mathbf{x}}$ direction (Fig. 3a). This remanent configuration indicates a minimization of the dipolar energy between contiguous regions and the existence of an effective anisotropy axis along the length of the zigzag pattern ($\hat{\mathbf{x}}$ axis). In fact, the average aspect ratio of the structure together with the magnetocrystalline anisotropy texture induced during sample fabrication can be responsible for this effective anisotropy.

Line scans perpendicular to the axis, along the $\hat{\mathbf{y}}$ axis (Fig. 3b), show the magnetization profile in a domain wall and at the centers of two contiguous parallelograms. The domain wall magnetization is relatively constant along the $\hat{\mathbf{x}}$ direction. However, in the parallelograms the angle of magnetization decays from $\pm 45^\circ$ at the edges to about $\pm 25^\circ$ in the middle of the structure. In order to model this numerically, the SEM topographic image of the structure was used as a template for a magnetization simulation with OOMMF, shown in Fig. 2b. The simulation was obtained using a 2-dimensional model with cell size of 10 nm x 10 nm and 30 nm thickness. Typical magnetic parameters for Permalloy films were used. Specifically, the magnetization was set to 800 $\times 10^3$ A/m, the exchange interaction was set to 13×10^{-12} J/m, and the magneto-crystalline anisotropy was varied from 0 to 1200 J/m^3. We found that the remanent state magnetization was relatively insensitive to the value of the anisotropy. The simulated data agree both qualitatively and quantitatively with the SEMPA data, as shown by the solid lines in Fig. 3.

The magnetoresistance of the structures was then measured at room temperature. The contacts, shown in Fig. 1, were designed to cover the ends of the element in order to eliminate the effects of the vortices. Figure 4 shows the experimental transfer curves of the structure measured for two orientations of the applied field, H. The dependence of the voltage V across the structure on H was measured for an applied current $I = 3$ mA. In the remanent state the zero-field voltage across the structure $V_o = 0.446$ V corresponds to a resistance $R_o = 149\ \Omega$.

For fields applied in the $\hat{\mathbf{x}}$ direction an antisymmetric transfer curve is observed. Figure 4a shows one branch of the hysterisis curve at low field. Following this branch down from the positive saturated state, the voltage across the structure decreases monotonically and reversibly to 0.45 % of its saturation value as the magnetization angles increase relative to

the current direction. This is followed by an irreversible jump at $|H| \approx 1$ kA·m^{-1}, where the domain walls change direction. For fields less than this value, we find that the transfer curves are completely reversible, with no evidence of minor loops even after many cycles. After jump, the voltage follows the opposite branch in the same fashion (see inset). The average sensitivity of the structure for a field range $\Delta H = 2$ kA·m^{-1} around zero is defined as $S_o = (\Delta V/\Delta H)\,(1/V_o)$ [9]. Therefore, for the parallel field configuration $S_o^{\parallel} = 3.54$ mV/(V·kA·m^{-1}).

For fields applied in the $\hat{\mathbf{y}}$ direction the transfer curve is comprised of two nearly symmetric flat branches near zero field. In the reversible region, shown in Fig. 4b, where $|H| \leq 1$ kA·m^{-1}, the voltage changes by only 0.05 % of the remanent value. This corresponds to a sensitivity $S_o^{\perp} = 0.31$ mV/(V·kA·m^{-1}) for a field range of $\Delta H = 2$ kA·m^{-1} around zero.

Therefore, these devices make highly directional low field sensors. Using the sensitivity values for H in the $\hat{\mathbf{y}}$ and $\hat{\mathbf{x}}$ directions, these sensors would have a rejection ratio, $r \equiv S_o^{\parallel}/S_o^{\perp}$, for H_y greater than 10. In addition, the inset Figure 4a shows that R_o is the same for both branches of the transfer curve, but the derivative with respect to H has different signs depending on which branch of the transfer curve the system is prepared [17]. This memory effect, combined with the fact that the device switches without forming minor loops, is scalable, and can be probed with very little power, shows that this device could also be useful as a cell in a magnetic random access memory (MRAM) device.

The remanent state image, (Fig. 2), shows that the magnetization is nearly uniform within the parallelogram regions. Also, the magnetization angle is correlated to the edge profile along the zigzag structure. This provides justification for a simple description of the system based on a pattern of alternating regions of single domain magnetizations that obey a coherent rotation model [18]. For simplicity, we assume that the regions do not interact. Therefore, only two representative regions are necessary to describe the zigzag structure. Each region will have a uniaxial easy axis pointing at an angle $\pm\psi_b$. The energy E_i of this system has the Zeeman and the uniaxial term for each region $i = 1,\ 2$. For an applied field H, we use the fact that the two regions are electrically connected in series to calculate the transfer curves based on the values of θ_i that minimize E_i.

The initial state of the system (at $H = 0$) is prepared with the $\hat{\mathbf{x}}-$component of the magnetization in each region pointing in the same direction. The values of θ_i that minimize E_i are used in conjunction with Eq. 1 to determine the behavior of the magnetoresistance of

the zigzag structure [9]. The parameters for the simulation are the zigzag angle ψ_b and the anisotropy field induced by the zigzag edge $H_k = 4$ kA·m^{-1}. The remaining magnetic and electric parameters are those of Permalloy [9]. The magnetoresistance curves for different values of ψ_b were then calculated and are shown in Fig. 5. For fields applied in the $\pm\hat{\mathbf{x}}$ direction, the magnetization in adjacent regions rotates in opposite directions, as illustrated in diagram shown in Fig. 5a. This forms a "scissors mode", where both angles either increase or decrease relative to the current direction. Therefore, the individual resistance changes add, and there is a net increase/decrease of the device resistance. Also, it can be seen in Fig. 5a that the sensitivity decreases with ψ_b, going to zero as ψ_b goes to zero.

For fields applied in the $\hat{\mathbf{y}}$ direction, we find a "rotation mode", where the magnetization in adjacent regions rotates in the same direction, as depicted in in the diagram of Fig. 5b. In this mode, the resistance changes tend to cancel each other out, resulting in a relatively flat, symmetric transfer curve. However, the sensitivity in the $\hat{\mathbf{y}}$ direction (Fig. 5b) vanishes at $\psi_b \approx 30°$. Therefore, the sensors are very directional for this value of ψ_b. In addition, we find excellent agreement between the calculated $\hat{\mathbf{y}}$ transfer curve at $\psi_b = 25°$ and the experimental data shown in Fig. 4(b). This is also corroborated by the SEMPA and OOMMF data of Fig. 3.

These results show that it is possible to naturally bias the magnetization in magnetoresistive sensors by choosing the appropriate contour of the magnetic element. In the particular case of a single layer MR sensor with a zigzag shape, the geometrical biasing mechanism works over a wide range of size scales, from the nanoscale region (width 250 nm), where it was originally reported, to the microscale (width 5 μm), where this study was conducted. This scaling should extend to small sizes until the distance between corners becomes comparable to the domain wall width in the magnetic material. We also find that modern computational models, such as OOMMF, can be used to understand and accurately predict the magnetic properties of devices at the nanoscale level. Based on the scalability and the fact that these elements can be described with a simple coherent rotation model, we expect this type of nano-engineering of the shape of the magnetic layer will have a significant impact in the areas of magnetic field sensors and memory applications.

Acknowledgments

We acknowledge support from NATO grant PST.CLG.979374. In addition, we would like to thank Alexander P. Popov, John N. Chapman, and Robert McMichael for useful discussions.

---

[1] M. Hermann, S. McVitie, and J.N. Chapman, J. Appl. Phys. **87**, 2994 (2000).

[2] M. Hermann PhD thesis, University of Glasgow (2000).

[3] J.C. Mallinson, Magneto-resistive and Spin-valve Heads, 2nd Ed., Academic Press (2002).

[4] P.I. Nikitin, S.I. Kasatkin, A.M. Muravjov, P.M. Vetoshko, M.V. Valeiko, V.I. Konov, and T. Meydan, Sens. Actuators A **106**, 26 (2003).

[5] S. Bae, K. Scheiman, W. Mertin, E. Kubalek, and M. Maywald, Microelectron. Reliab. **39**, 975 (1999).

[6] B.D. Schrag, Gang Xiao, Appl. Phys. Lett. **82**(19), 3272 (2003).

[7] S. Tumański and A. Liszka, J. Magn. Magn. Mater. **242−245**, 1253 (2002).

[8] P.L. Rossiter, The Electrical Resistivity of Metals and Alloys, Cambridge University Press (1987).

[9] See, for example, U. Dibbern in Sensors a Comprehensive Survey, Ch. 9, Edited by R. Boll and K.J. Overshott, VCH Publishers Inc. (1989).

[10] S. Tumański and M Stabrowski, Sens. Actuators **7**, 285 (1985).

[11] K.J. Kirk, J.N. Chapman, and C.D.W. Wilkinson, Appl. Phys. Lett. **71**, 539 (1997).

[12] M.R. Scheinfein, J. Unguris, M.H. Kelley, D.T. Pierce, and R.J. Celotta, Rev. Sci. Instrum. **61**, 2501 (1990).

[13] Scanning Electron Microscopy with Polarization Analysis (SEMPA) and its Applications, J. Unguris, Magnetic Imaging and its Applications to Materials, eds. M. de Graef and Y. Zhu, Burlington, MA:Academic Press, 2000, p. 167-303(2000).

[14] M.J. Donahue and D.J. Porter, OOMMF's User Guide, Version 1.0, NISTIR 6376, National Institute of Standards and Technology, Gaithersburg, MD (Sept. 1999). For more information, see website at http://math.nist.gov/oommf/

[15] W. F. Brown, Jr., Micromagnetics (Interscience, New York, 1963).

[16] J. Fidler and T. Schrefl, "Micromagnetic modelling - the current state of the art," J PHYS D APPL PHYS 33 (15): R135-R156 AUG 7 2000.

[17] J. Aumentado and V. Chandrasekhar, Appl. Phys. Lett. **74**, 1898 (1999).

[18] E.C. Stoner and E.P. Wohlfarth, Phil. Trans. R. Soc. London A **240**, 599 (1948).

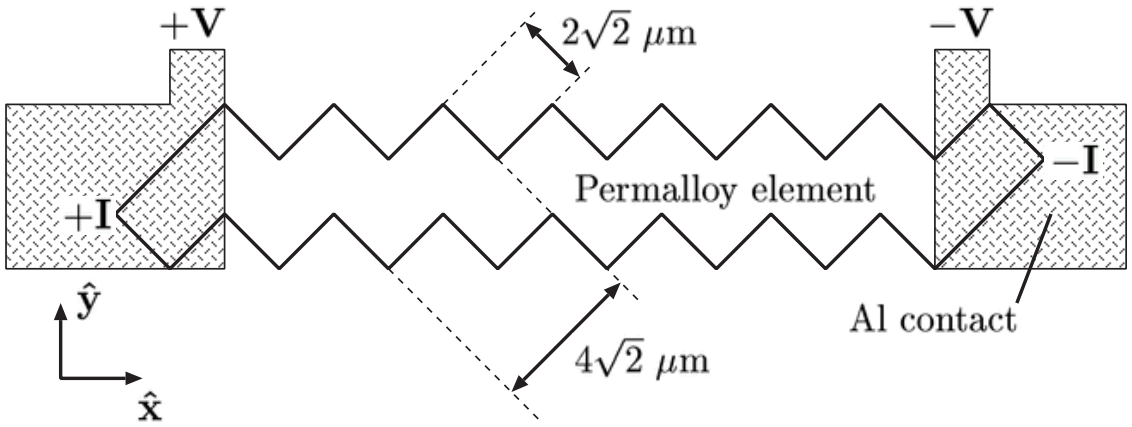

FIG. 1: Diagram showing the dimensions and electrical contacts of the zigzag structure. They are parameterized using a rectangular building block with lateral dimensions $2\sqrt{2}$ μm $\times$ $4\sqrt{2}$ μm. An 8-block zigzag pattern was fabricated. The structure is 35 μm long and 5 μm wide.

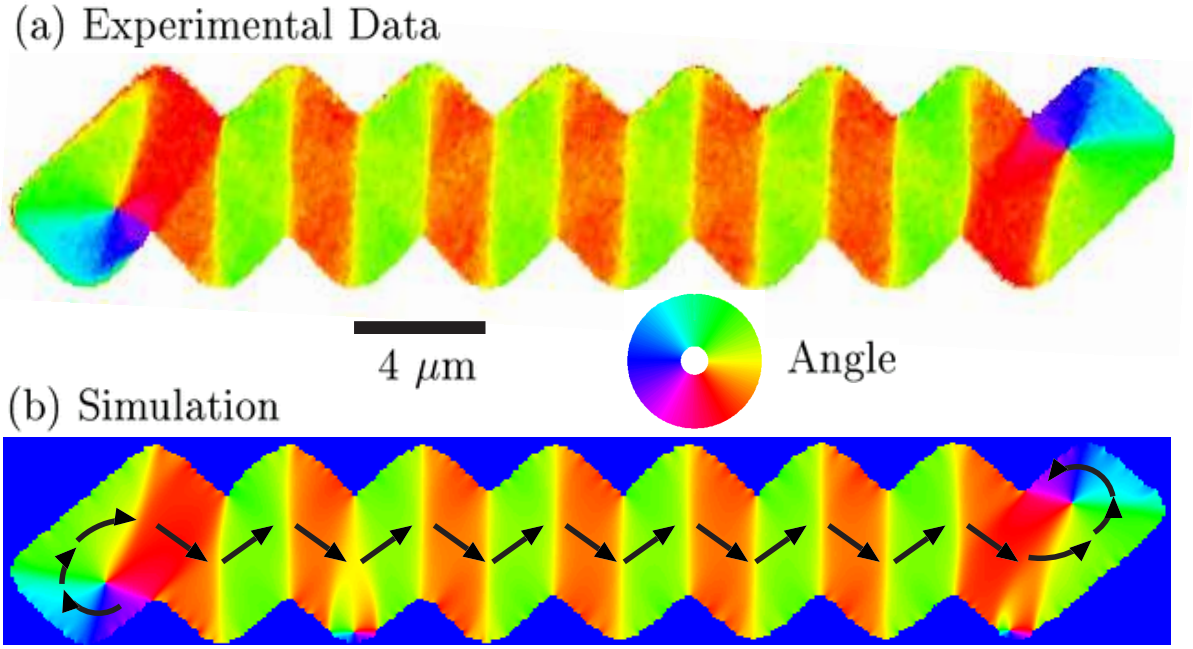

FIG. 2: (a) Experimental SEMPA image of the 8-block zigzag structure. (b) Simulation performed on the same geometry using OOMMF. The magnetization direction maps onto the angle color map ring.

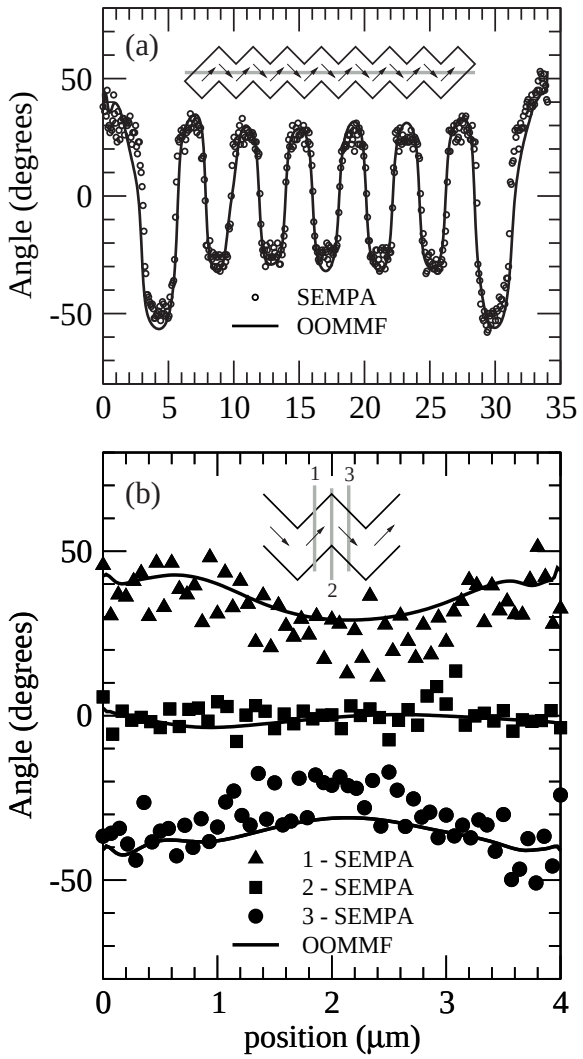

FIG. 3: Magnetization line scan from the SEMPA data and OOMMF simulation along (a) $\hat{\mathbf{x}}$ and (b) $\hat{\mathbf{y}}$ directions. The uncertainty in the SEMPA data is 5°, as seen by scatter in the data.

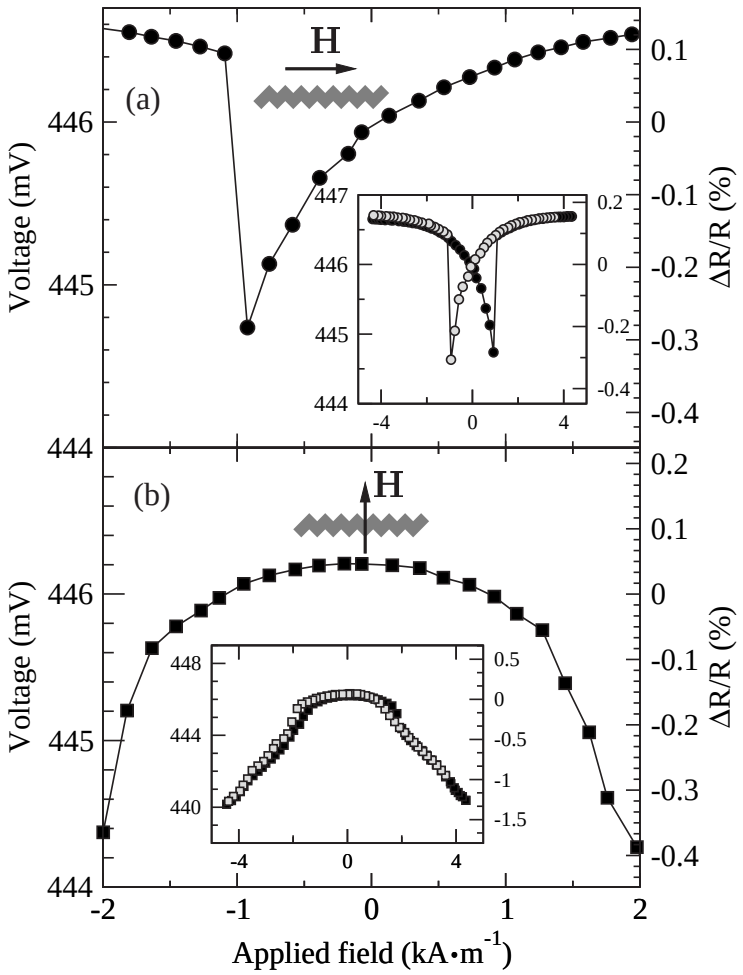

FIG. 4: Transfer curves of the 8-block zigzag structure measured for applied field in (a) the $\hat{\mathbf{x}}$ direction and (b) the $\hat{\mathbf{y}}$ direction. The insets show both branches of the transfer curve at higher fields.

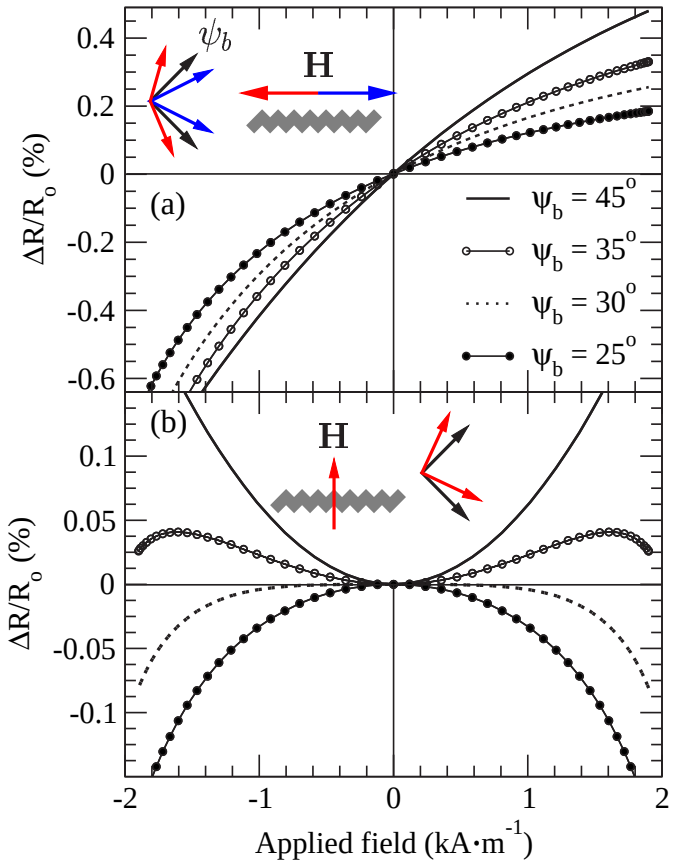

FIG. 5: Simulated transfer curves obtained using the single domain coherent rotation model with the applied field along the (a) $\hat{\mathbf{x}}$ and (b) $\hat{\mathbf{y}}$ directions. Top diagram shows the scissor mode and bottom diagram shows the rotation mode.